Anderson-Bogoliubov and Carlson-Goldman modes in counterflow superconductors: Case study of a double monolayer graphene

K. V. Germash[1] and D. V. Fil[1,2,*]

[1]*Institute for Single Crystals, National Academy of Sciences of Ukraine, 60 Nauky Avenue, Kharkiv 61072, Ukraine*

[2]*V.N. Karazin Kharkiv National University, 4 Svobody Square, Kharkiv 61022, Ukraine*

(Received 7 December 2018; published 11 March 2019)

The impact of electron-hole pairing on the spectrum of plasma excitations in double layer systems is investigated. The theory is developed with reference to a double monolayer graphene. Taking into account the coupling of scalar potential oscillations with oscillations of the order parameter Δ, we show that the spectrum of antisymmetric (acoustic) plasma excitations contains two modes: a weakly damped mode below the gap 2Δ and a strongly damped mode above the gap. The lower mode can be interpreted as an analog of the Carlson-Goldman mode. This mode has an acoustic dispersion relation at small wave vectors and it saturates at the level 2Δ at large wave vectors. Its velocity is larger than the velocity of the Anderson-Bogoliubov mode $v_{AB} = v_F/\sqrt{2}$, and it can be smaller than the Fermi velocity v_F. The damping rate of this mode strongly increases under increase of temperature. Out-of-phase oscillations of two order parameters in two spin subsystems are also considered. This part of the spectrum contains two more modes. One of them is interpreted as an analog of the Anderson-Bogoliubov (phase) mode and the other as an analog of the Schmid (amplitude) mode. With minor modifications the theory can be extended to describe collective modes in a double bilayer graphene as well.

DOI: 10.1103/PhysRevB.99.125412

I. INTRODUCTION

Electron-hole pairing is a phenomenon analogous to the Cooper pairing that may occur in double layer systems consisting of an electron-doped layer and a hole-doped layer [1,2] (see also Ref. [3] for a review). In the paired state the system may support dissipationless counterflow—a flow of oppositely directed superconducting electric currents in adjacent layers. The phenomenon is referred to as the superfluidity of spatially indirect excitons, exciton condensation in bilayers, or the counterflow superconductivity.

A strong increase of the counterflow conductivity at low temperature caused by the electron-hole pairing was observed [4–6] in quantum Hall bilayers with the total filling factor of 1 [$\nu_T = 2\pi\ell_B^2(n_1 + n_2) = 1$, where n_i is the electron density in the ith layer and ℓ_B is the magnetic length]. The current state of art in experimental investigations of exciton condensation in $\nu_T = 1$ quantum Hall bilayers is described in Ref. [7]. Quantum Hall bilayers demonstrate a zero bias peak in the differential tunneling conductance [8] and a strong interlayer drag resistance [9]. These two features are considered as experimental signatures of the electron-hole pairing. Similar features were observed in double layer systems in zero magnetic field. The increase of the interlayer drag resistance at low temperature was detected in a double quantum well in AlGaAs heterostructures [10,11] and in hybrid double layer systems comprising a monolayer (bilayer) graphene in close proximity to a quantum well created in GaAs [12]. Experimental observation of strongly enhanced tunneling between two graphene bilayers at equal occupation of adjacent bilayers by electrons and holes was reported recently [13]. The registered tunneling conductance at small bias voltage was many orders of magnitude greater than that predicted for uncorrelated electrons and holes.

Theoretical consideration shows that promising candidates for a realization of electron-hole pairing in zero magnetic field are double monolayer [14–19], double bilayer [20–22], and double multilayer [23] graphenes, double transition metal dichalcogenide monolayers [24–26], a phosphorene double layer [27,28], and topological insulators [29,30].

In recent papers [31–33] we have predicted the effects that can be considered as additional hallmarks of the electron-hole pairing. It was shown [31] that the electron-hole pairing suppresses the ability of a double layer graphene system to screen the electrostatic field of an external charge. In the paired state at $T = 0$ the electrostatic field remains completely unscreened at large distances. It was found [32] that the electron-hole pairing influences significantly the spectrum of plasma excitations in a double layer graphene system. Namely, instead of one optical (symmetric) plasmon mode two symmetric modes emerge. The frequency of the lower mode is restricted from above by the inequality $\hbar\omega < 2\Delta$, where 2Δ is the gap in the electron spectrum caused by the electron-hole pairing. This mode is a weakly damped one and its frequency is very sensitive to the temperature. At $T = 0$ the lower mode disappears. In contrast, the upper mode belongs to the frequency domain $\hbar\omega > 2\Delta$, it is strongly damped mode, its frequency is less sensitive to the temperature, and it survives at $T = 0$. It was also established [33] that the electron-hole pairing provokes a huge increase of efficiency of the third-harmonic generation in double monolayer and double bilayer graphenes.

*fil@isc.kharkov.ua

The results [31–33] were obtained within an approach that does not account for the oscillations of the order parameter of the electron-hole pairing. It is known from the Bardeen-Cooper-Schrieffer (BCS) theory of superconductivity [34,35] that neglecting the order parameter oscillations results in a violation of the gauge invariancy of the polarization matrix. The gauge invariance is restored by "dressing" of the vertexes. The "dressed" vertexes should satisfy the generalized Ward identity. In Ref. [32] we proposed a heuristic approach to the problem. We obtained the gauge invariant polarization matrix using the vertex functions obtained as particular solutions of the generalized Ward identity.

In this paper we present an approach in which the order parameter oscillations are accounted for explicitly. Our approach is close to one developed in Ref. [36] for conventional superconductors.

In Sec. II we introduce the model, in which the electron-hole pairing is described by the order parameter, which is independent of the momenta of paired quasiparticles. The perturbation Hamiltonian that accounts for the order parameter oscillations is given in Sec. III. In Sec. IV the analytical expressions for the response functions and the polarization matrix are obtained. In Sec. V we derive the dispersion equation and calculate the eigenmode spectrum. We identify six modes. Two modes correspond to in-phase oscillations of the scalar potentials of two layers. It reproduces the result of Ref. [32]. Two other modes correspond to out-of-phase oscillations of the scalar potentials coupled to in-phase oscillations of two order parameters (two order parameters describe pairing in two spin subsystems). One of these modes is interpreted as an analog of the Carlson-Goldman mode in superconductors. The remaining two modes correspond to out-of-phase oscillations of two order parameters. They can be considered as analogs of the Anderson-Bogoliubov (phase) and Schmid (amplitude) modes in neutral superfluids and superconductors.

II. THE MODEL

We consider the electron-hole pairing in a double monolayer graphene system where the concentration of electrons in one layer is equal to the concentration of holes in the other layer. We specify the case of two graphene layers with zero relative twist. The graphene layers are separated by a dielectric layer with the dielectric constant ε and surrounded by a medium with $\varepsilon = 1$. The hopping between graphene layers is neglected.

We describe the pairing by the order parameter, which is independent of the momentum. Such an order parameter can be defined self-consistently in the case of contact interaction between electrons and holes [16,17]. In the model with contact interaction the problem of finding the collective mode spectrum can be reduced to a set of algebraic equations (in the general case for the momentum-dependent order parameter the algebraic equations are transformed into integral ones).

We describe the system by the Hamiltonian

$$H = H_1 + H_2 + H_{12}, \tag{1}$$

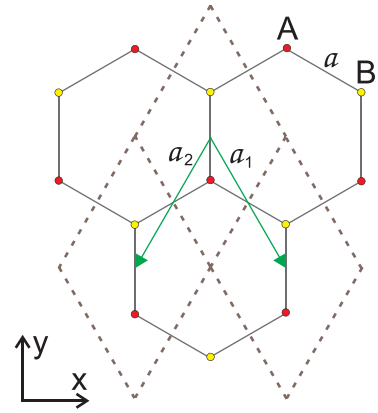

FIG. 1. Graphene lattice. The red (dark) and yellow (light) circles correspond to the A and B sublattices. The unit cells are shown by dashed lines and two primitive lattice vectors are shown by arrows.

where

$$H_n = -t \sum_{\sigma} \sum_{i} \sum_{j=1,2,3} (c^{+}_{n,i,A,\sigma} c_{n,i+\delta_j,B,\sigma} + \text{H.c.}) - \mu_n \sum_{i,\sigma} \sum_{\alpha} c^{+}_{n,i,\alpha,\sigma} c_{n,i,\alpha,\sigma} \tag{2}$$

is the single-layer Hamiltonian, $c^{+}_{n,i,\alpha,\sigma}$ and $c_{n,i,\alpha,\sigma}$ are the creation and annihilation operators of electrons, $n = 1, 2$ is the layer index, i is the unit cell index, $\alpha = A, B$ is the sublattice index, $\sigma = \uparrow, \downarrow$ is the spin index, t is the nearest-neighbor hopping energy, μ_n is the electron chemical potential in the nth layer, and the index $i + \delta_j$ stands for the unit cell with the coordinate $\mathbf{R}_i + \boldsymbol{\delta}_j$. Here $\mathbf{R}_i$ is the radius vector of the ith unit cell, vectors $(\boldsymbol{\delta}_1, \boldsymbol{\delta}_2, \boldsymbol{\delta}_3) = (0, \mathbf{a}_1, \mathbf{a}_2)$ connect a given unit cell with unit cells where the nearest-neighbor B sites are located, $\mathbf{a}_{1(2)} = (\pm\sqrt{3}a/2, -3a/2)$ are the primitive lattice vectors, and a is the distance between the nearest-neighbor atoms in graphene (see Fig. 1).

The chemical potentials are counted from the Dirac points and satisfy the condition $\mu_1 = -\mu_2 = \mu$ that corresponds to equal concentrations of electrons and holes. The interaction part of the Hamiltonian reads

$$H_{12} = V \sum_{i,\alpha,\sigma} c^{+}_{1,i,\alpha,\sigma} c^{+}_{2,i,\alpha,\sigma} c_{2,i,\alpha,\sigma} c_{1,i,\alpha,\sigma}, \tag{3}$$

where V is the interaction constant ($V > 0$).

The order parameter of the electron-hole pairing is defined as

$$\Delta_{i,\alpha,\sigma} = V \langle c^{+}_{2,i,\alpha,\sigma} c_{1,i,\alpha,\sigma} \rangle. \tag{4}$$

The order parameter can be presented as a sum of the equilibrium part $\Delta^{(0)}_{i,\alpha,\sigma}$ and the fluctuating part $\Delta^{(fl)}_{i,\alpha,\sigma}(t)$. We consider the paired state with the lowest energy [16,17] that corresponds to the choice $\Delta^{(0)}_{i,A,\sigma} = -\Delta^{(0)}_{i,B,\sigma} = \Delta$. The property $\Delta_{i,A} = -\Delta_{i,B}$ provides the opening of the gap in the quasiparticle spectrum. The contact interaction model with $\Delta_{i,A} = -\Delta_{i,B}$ [16,17] and the model based on a treatment of the long-range Coulomb interaction (bare or screened) [14,15,18,19] give similar results. In addition, keeping in

mind that in the Dirac approximation the conduction-band and valence-band states are described by the sublattice spinors $(1/\sqrt{2}, e^{i\theta_{\mathbf{k}}}/\sqrt{2})$ and $(1/\sqrt{2}, -e^{i\theta_{\mathbf{k}}}/\sqrt{2})$ respectively ($\hbar\mathbf{k}$ is momentum measured from the Dirac point and $\theta_{\mathbf{k}}$ is the angular orientation of this momentum), one can see [17] that the order parameter with $\Delta_{i,A} = -\Delta_{i,B}$ couples the conduction-band and valence-band states with equal strength at all $\theta_{\mathbf{k}}$.

Neglecting the order parameter oscillations we obtain the mean-field Hamiltonian

$$H_{MF} = H_1 + H_2 - \sum_{i,\sigma}(\Delta c^{+}_{1,i,A,\sigma} c_{2,i,A,\sigma} - \Delta c^{+}_{1,i,B,\sigma} c_{2,i,B,\sigma} + \text{H.c.}). \tag{5}$$

Applying the Fourier transformation to the Hamiltonian (5) and considering one spin component, we get

$$H_{MF} = \sum_{\mathbf{k}} \Psi^{+}_{\mathbf{k}} h_{\mathbf{k}} \Psi_{\mathbf{k}} = \sum_{\mathbf{k}} (c^{+}_{1,A,\mathbf{k}}\ c^{+}_{1,B,\mathbf{k}}\ c^{+}_{2,A,\mathbf{k}}\ c^{+}_{2,B,\mathbf{k}}) \times \begin{pmatrix} -\mu & f_{\mathbf{k}} & -\Delta & 0 \\ f^{*}_{\mathbf{k}} & -\mu & 0 & \Delta \\ -\Delta & 0 & \mu & f_{\mathbf{k}} \\ 0 & \Delta & f^{*}_{\mathbf{k}} & \mu \end{pmatrix} \begin{pmatrix} c_{1,A,\mathbf{k}} \\ c_{1,B,\mathbf{k}} \\ c_{2,A,\mathbf{k}} \\ c_{2,B,\mathbf{k}} \end{pmatrix}, \tag{6}$$

where $c_{n,A(B),\mathbf{k}} = (1/\sqrt{N}) \sum_i c_{n,i,A(B)} e^{-i\mathbf{k}\mathbf{R}_i}$ is the Fourier-transformed annihilation operator, N is the total number of unit cells and the creation operator is given by the Hermitian conjugate, and $f_{\mathbf{k}} = |f_{\mathbf{k}}| e^{i\chi_{\mathbf{k}}} = -t \sum_{j=1,2,3} \exp(i\mathbf{k}\boldsymbol{\delta}_j)$. Here we omit the spin index.

The Hamiltonian (6) is diagonalized by the unitary transformation

$$H_{MF} = \sum_{\mathbf{k}} \Psi^{+}_{\mathbf{k}} \hat{U}^{-1}_{\mathbf{k}} \hat{U}_{\mathbf{k}} h_{\mathbf{k}} \hat{U}^{-1}_{\mathbf{k}} \hat{U}_{\mathbf{k}} \Psi_{\mathbf{k}} = \sum_{\mathbf{k}} \tilde{\Psi}^{+}_{\mathbf{k}} \tilde{h}_{\mathbf{k}} \tilde{\Psi}_{\mathbf{k}}, \tag{7}$$

where $\tilde{h}_{\mathbf{k}} = \hat{U}_{\mathbf{k}} h_{\mathbf{k}} \hat{U}^{-1}_{\mathbf{k}}$ and $\tilde{\Psi}_{\mathbf{k}} = \hat{U}_{\mathbf{k}} \Psi_{\mathbf{k}}$. The matrix $\hat{U}_{\mathbf{k}}$ can be written in a form of the product

$$\hat{U}_{\mathbf{k}} = \hat{U}_{uv} \hat{U}_b \hat{U}_{\chi}. \tag{8}$$

The matrix

$$\hat{U}_{\chi} = \frac{1}{\sqrt{2}} \begin{pmatrix} 1 & e^{i\chi_{\mathbf{k}}} & 0 & 0 \\ 1 & -e^{i\chi_{\mathbf{k}}} & 0 & 0 \\ 0 & 0 & 1 & e^{i\chi_{\mathbf{k}}} \\ 0 & 0 & 1 & -e^{i\chi_{\mathbf{k}}} \end{pmatrix} \tag{9}$$

diagonalizes the single-layer parts of the Hamiltonian. The matrix

$$\hat{U}_b = \begin{pmatrix} 1 & 0 & 0 & 0 \\ 0 & 0 & 0 & 1 \\ 0 & 1 & 0 & 0 \\ 0 & 0 & 1 & 0 \end{pmatrix} \tag{10}$$

rearranges the elements of the matrix $\hat{U}_{\chi} h_{\mathbf{k}} \hat{U}^{-1}_{\chi}$ into two blocks:

$$\hat{U}_b \hat{U}_{\chi} h_{\mathbf{k}} \hat{U}^{-1}_{\chi} \hat{U}^{-1}_b = \begin{pmatrix} \xi_{\mathbf{k},+1} & -\Delta & 0 & 0 \\ -\Delta & -\xi_{\mathbf{k},+1} & 0 & 0 \\ 0 & 0 & \xi_{\mathbf{k},-1} & -\Delta \\ 0 & 0 & -\Delta & -\xi_{\mathbf{k},-1} \end{pmatrix}, \tag{11}$$

where $\xi_{\mathbf{k},\lambda} = \lambda|f_{\mathbf{k}}| - \mu$ is the electron spectrum of a single graphene layer, and $\lambda = \pm 1$ corresponds to the conduction (valence) band.

Each block can be diagonalized by the u-v transformation. The matrix

$$\hat{U}_{uv} = \begin{pmatrix} u_{\mathbf{k},+1} & -v_{\mathbf{k},+1} & 0 & 0 \\ v_{\mathbf{k},+1} & u_{\mathbf{k},+1} & 0 & 0 \\ 0 & 0 & u_{\mathbf{k},-1} & -v_{\mathbf{k},-1} \\ 0 & 0 & v_{\mathbf{k},-1} & u_{\mathbf{k},-1} \end{pmatrix} \tag{12}$$

is expressed through the coefficients of this transformation:

$$u_{\mathbf{k},\lambda} = \sqrt{\frac{1}{2}\left(1 + \frac{\xi_{\mathbf{k},\lambda}}{E_{\mathbf{k},\lambda}}\right)}, \quad v_{\mathbf{k},\lambda} = \sqrt{\frac{1}{2}\left(1 - \frac{\xi_{\mathbf{k},\lambda}}{E_{\mathbf{k},\lambda}}\right)}, \tag{13}$$

where $E_{\mathbf{k},\lambda} = \sqrt{\xi^2_{\mathbf{k},\lambda} + \Delta^2}$.

The transformed Hamiltonian has the diagonal form

$$H_{MF} = \sum_{\nu} E_{\nu} \alpha^{+}_{\nu} \alpha_{\nu}, \tag{14}$$

where $\nu = (\mathbf{k}, \lambda, m)$ is the full set of the quasiparticle quantum numbers, excluding spin, $E_{\nu} = mE_{\mathbf{k},\lambda}$ is the quasiparticle energy, $m = \pm 1$ corresponds to the states above (below) the gap, and α^{+}_{ν}, α_{ν} are the quasiparticle creation and annihilation operators.

Applying to Eq. (4) the Fourier-transformation and the unitary transformation $\hat{U}_{\mathbf{k}}$, we obtain the following equation for the order parameter:

$$\Delta = -\frac{V}{2N} \sum_{\nu} m u_{\mathbf{k},\lambda} v_{\mathbf{k},\lambda} \langle \alpha^{+}_{\nu} \alpha_{\nu} \rangle. \tag{15}$$

Replacing the average $\langle \alpha^{+}_{\nu} \alpha_{\nu} \rangle$ with the Fermi distribution function and calculating the sum over m, we arrive at the self-consistence equation

$$\Delta = \frac{V\Omega_0}{2S} \sum_{\mathbf{k},\lambda} \frac{\Delta}{2E_{\mathbf{k},\lambda}} \tanh \frac{E_{\mathbf{k},\lambda}}{2T}, \tag{16}$$

where Ω_0 is the area of the unit cell and S is the area of the system.

We emphasize that Eq. (16) differs from one obtained in the model with a long-range Coulomb interaction [14,15,18,19]. In the latter case the self-consistence equation has the form

$$\Delta_{\mathbf{k},\lambda} = \frac{1}{S} \sum_{\mathbf{k}',\lambda'} V(\mathbf{k} - \mathbf{k}') \frac{1 + \lambda\lambda' \cos(\chi_{\mathbf{k}} - \chi_{\mathbf{k}'})}{2} \frac{\Delta_{\mathbf{k}',\lambda'}}{2E_{\mathbf{k}',\lambda'}} \times \tanh \frac{E_{\mathbf{k}',\lambda'}}{2T}, \tag{17}$$

where $V(\mathbf{q})$ is the Fourier component of the interlayer Coulomb interaction. Differently from Eq. (16), the order parameter independent of $\mathbf{k}$ and λ does not satisfy Eq. (17).

III. PERTURBATION HAMILTONIAN

Now we add to the Hamiltonian (6) the perturbation part H_{int}. The perturbation Hamiltonian H_{int} describes the oscillations of the order parameter and the interaction of electrons with the scalar potential $\varphi(\mathbf{r}, t)$. We consider the oscillations

for which $\Delta^{(fl)}_{i,A,\sigma}(t) = -\Delta^{(fl)}_{i,B,\sigma}(t) = \Delta^{(fl)}_{i,\sigma}(t)$ and do not take into account oscillations with $\Delta^{(fl)}_{i,A,\sigma} = +\Delta^{(fl)}_{i,B,\sigma}$. The latter ones are decoupled from the scalar potential oscillations and do not modify the response to the electromagnetic field.

The Fourier components of the real and imaginary parts of the order parameter oscillations are defined as

$$\Delta_1(\mathbf{q},\omega) = \Omega_0 \sum_i \int dt\, e^{i\omega t - i\mathbf{q}\mathbf{R}_i}\, \mathrm{Re}\big[\Delta^{(fl)}_i(t)\big], \tag{18}$$

$$\Delta_2(\mathbf{q},\omega) = \Omega_0 \sum_i \int dt\, e^{i\omega t - i\mathbf{q}\mathbf{R}_i}\, \mathrm{Im}\big[\Delta^{(fl)}_i(t)\big]. \tag{19}$$

We specify the case of real-valued Δ [it is accounted for in the Hamiltonian (6) and in the coefficients (13)]. Then the quantities Δ_1 and Δ_2 describe small oscillations of the amplitude and the phase of the order parameter, respectively.

The perturbation Hamiltonian can be presented in the matrix form

$$H_{\mathrm{int}}(t) = -\frac{1}{2\pi S}\sum_{\mathbf{k},\mathbf{q}}\int d\omega\, e^{-i\omega t}\Psi^{+}_{\mathbf{k}+\mathbf{q}}\Big[\frac{e}{2}\varphi_{+}(\mathbf{q},\omega)\hat{T}^{(0)} + \Delta_1(\mathbf{q},\omega)\hat{T}^{(1)} + \Delta_2(\mathbf{q},\omega)\hat{T}^{(2)} + \frac{e}{2}\varphi_{-}(\mathbf{q},\omega)\hat{T}^{(3)}\Big]\Psi_{\mathbf{k}}, \tag{20}$$

where the operators $\Psi^{+}_{\mathbf{k}}$ and $\Psi_{\mathbf{k}}$ are defined by Eq. (6),

$$\varphi_{\pm}(\mathbf{q},\omega) = \Omega_0 \sum_i \int dt\, e^{i\omega t - i\mathbf{q}\mathbf{R}_i}[\varphi_1(\mathbf{R}_i,t) \pm \varphi_2(\mathbf{R}_i,t)] \tag{21}$$

is the Fourier-component of the sum (difference) of the scalar potentials in two graphene layers, and $\varphi_n(\mathbf{R}_i,t)$ is the scalar potential in the nth layer in the ith unit cell. The matrices $\hat{T}^{(s)}$ in Eq. (20) are expressed through the Pauli matrix $\hat{\sigma}_z$ and the identity matrix $\hat{I}$:

$$\hat{T}^{(0)} = \begin{pmatrix}\hat{I} & 0\\ 0 & \hat{I}\end{pmatrix},\quad \hat{T}^{(1)} = \begin{pmatrix}0 & \hat{\sigma}_z\\ \hat{\sigma}_z & 0\end{pmatrix},$$
$$\hat{T}^{(2)} = \begin{pmatrix}0 & i\hat{\sigma}_z\\ -i\hat{\sigma}_z & 0\end{pmatrix},\quad \hat{T}^{(3)} = \begin{pmatrix}\hat{I} & 0\\ 0 & -\hat{I}\end{pmatrix}. \tag{22}$$

We apply the transformation (7) to the Hamiltonian (20) and write it through the operators of creation and annihilation of quasiparticle excitations:

$$H_{\mathrm{int}}(t) = \frac{1}{2\pi S}\sum_{\nu_1,\nu_2}\int d\omega\, e^{-i\omega t}\alpha^{+}_{\nu_1}[h_{\mathrm{int}}(\omega)]_{\nu_1,\nu_2}\alpha_{\nu_2}, \tag{23}$$

where

$$[h_{\mathrm{int}}(\omega)]_{\nu_1,\nu_2} = -\frac{e}{2}\varphi_{+}(\mathbf{k}_2-\mathbf{k}_1,\omega)R^{(0)}_{\nu_1,\nu_2} - \Delta_1(\mathbf{k}_2-\mathbf{k}_1,\omega)\times R^{(1)}_{\nu_1,\nu_2} - \Delta_2(\mathbf{k}_2-\mathbf{k}_1,\omega)R^{(2)}_{\nu_1,\nu_2} - \frac{e}{2}\varphi_{-}(\mathbf{k}_2-\mathbf{k}_1,\omega)R^{(3)}_{\nu_1,\nu_2}, \tag{24}$$

the matrices $R^{(s)}_{\nu_1,\nu_2}$ $(s = 0, 1, 2, 3)$ are given by the equation

$$R^{(s)}_{\mathbf{k}_1,\lambda_1,m_1;\mathbf{k}_2,\lambda_2,m_2} = \frac{1+\lambda_1\lambda_2 e^{i(\chi_{\mathbf{k}_1}-\chi_{\mathbf{k}_2})}}{2}\times[M^{(s)}(\mathbf{k}_1,\lambda_1,\mathbf{k}_2,\lambda_2)]_{i_{m_1},i_{m_2}}, \tag{25}$$

$(i_{+1}\equiv 1,\ i_{-1}\equiv 2)$, and the matrices $\hat{M}^{(s)}$ are expressed through the product

$$\hat{M}^{(s)}(\mathbf{k}_1,\lambda_1,\mathbf{k}_2,\lambda_2) = \begin{pmatrix}u_{\mathbf{k}_1,\lambda_1} & -v_{\mathbf{k}_1,\lambda_1}\\ v_{\mathbf{k}_1,\lambda_1} & u_{\mathbf{k}_1,\lambda_1}\end{pmatrix}\hat{\sigma}^{(s)}\times\begin{pmatrix}u_{\mathbf{k}_2,\lambda_2} & v_{\mathbf{k}_2,\lambda_2}\\ -v_{\mathbf{k}_2,\lambda_2} & u_{\mathbf{k}_2,\lambda_2}\end{pmatrix} \tag{26}$$

with $\hat{\sigma}^{(0)} = \hat{I}$, $\hat{\sigma}^{(1)} = \hat{\sigma}_x$, $\hat{\sigma}^{(2)} = -\hat{\sigma}_y$, $\hat{\sigma}^{(3)} = \hat{\sigma}_z$.

IV. POLARIZATION MATRIX

Taking into account two spin components, we write the Hamiltonian in the form

$$H(t) = H_{MF} + H_{\mathrm{int}}(t) = \sum_{\nu,\sigma}E_\nu\alpha^{+}_{\nu,\sigma}\alpha_{\nu,\sigma} + \frac{1}{2\pi S}\times\sum_{\nu_1,\nu_2,\sigma}\int d\omega\, e^{-i\omega t}\alpha^{+}_{\nu_1,\sigma}[h_{\mathrm{int},\sigma}(\omega)]_{\nu_1,\nu_2}\alpha_{\nu_2,\sigma}, \tag{27}$$

where $[h_{\mathrm{int},\sigma}(\omega)]_{\nu_1,\nu_2}$ is given by Eq. (24) with $\Delta_{1(2)}(\mathbf{k},\omega)\equiv\Delta_{1(2),\sigma}(\mathbf{k},\omega)$.

To calculate the response of the system to the scalar potential and to the order parameter oscillations, we define the response functions

$$\eta^{(s)}_{\sigma}(\mathbf{q},\omega) = \int dt\, e^{i\omega t}\sum_{\mathbf{k}}\langle\Psi^{+}_{\mathbf{k}-\mathbf{q},\sigma}\hat{T}^{(s)}\Psi_{\mathbf{k},\sigma}\rangle, \tag{28}$$

where $\Psi^{+}_{\mathbf{k},\sigma}$ and $\Psi_{\mathbf{k},\sigma}$ are the same operators as in Eq. (6) with restored spin indexes. The angle brackets mean the quantum mechanical and thermodynamic average. We compute the averages in Eq. (28) using the density matrix formalism. The density matrix $\hat{\rho}(t)$ satisfies the equation

$$\frac{\partial\hat{\rho}(t)}{\partial t} = \frac{1}{i\hbar}[H(t),\hat{\rho}(t)] - \gamma(\hat{\rho}(t)-\hat{\rho}_0), \tag{29}$$

where $\hat{\rho}_0$ is the density matrix of the system described by the Hamiltonian H_{MF}, and γ is the relaxation rate. The quantity γ is the phenomenological parameter. In what follows we consider small γ $(\hbar\gamma \ll \mu)$. It corresponds to the pure limit. Accounting for the term with γ in Eq. (29) allows to calculate numerically the integrals in the expressions for the polarization matrix and to evaluate the Landau damping.

The averages in Eq. (28) are calculated as

$$\langle\Psi^{+}_{\mathbf{k}-\mathbf{q},\sigma}\hat{T}^{(s)}\Psi_{\mathbf{k},\sigma}\rangle = \mathrm{Tr}\big([\hat{\rho}(t)]_{\mathbf{k},\sigma;\mathbf{k}-\mathbf{q},\sigma}\hat{T}^{(s)}\big), \tag{30}$$

where the trace is taken over the sublattice and layer indexes.

In the quasiparticle basis the response functions (28) are expressed as

$$\eta^{(s)}_{\sigma}(\mathbf{q},\omega) = \sum_{\nu_1,\nu_2}[\hat{\rho}(\omega)]_{\nu_1,\sigma;\nu_2,\sigma}R^{(s)}_{\nu_2,\nu_1}\delta_{\mathbf{k}_1-\mathbf{q},\mathbf{k}_2}, \tag{31}$$

where $\hat{\rho}(\omega) = \int dt\,\exp(i\omega t)\hat{\rho}(t)$ and the matrixes $R^{(s)}_{\nu_1,\nu_2}$ are given by Eq. (25).

The density matrix is sought in a form of expansion in powers of the perturbation Hamiltonian: $\hat{\rho}(\omega) = \hat{\rho}_0(\omega) + \hat{\rho}_1(\omega) + \cdots$. The zero-order term in this expansion is the equilibrium density matrix

$$[\hat{\rho}_0(\omega)]_{\nu_1,\sigma_1;\nu_2,\sigma_2} = 2\pi\delta(\omega)\delta_{\nu_1,\nu_2}\delta_{\sigma_1,\sigma_2}f_{\nu_1}, \tag{32}$$

where $f_\nu = (e^{E_\nu/T}+1)^{-1}$ is the Fermi distribution function. The first-order term reads

$$[\hat{\rho}_1(\omega)]_{\nu_1,\sigma_1;\nu_2,\sigma_2} = \frac{1}{S}\frac{f_{\nu_1}-f_{\nu_2}}{E_{\nu_1}-E_{\nu_2}-\hbar(\omega+i\gamma)} \times [h_{\mathrm{int},\sigma_1}(\omega)]_{\nu_1,\nu_2}\delta_{\sigma_1,\sigma_2}. \tag{33}$$

The response functions $\eta^{(0)}$ and $\eta^{(3)}$ at $\mathbf{q}\neq 0$ correspond to the charge density oscillations $\rho_{\pm,\sigma} = \rho_{1,\sigma} \pm \rho_{2,\sigma}$:

$$\rho_{+,\sigma}(\mathbf{q},\omega) = -e\eta^{(0)}_\sigma(\mathbf{q},\omega), \quad \rho_{-,\sigma}(\mathbf{q},\omega) = -e\eta^{(3)}_\sigma(\mathbf{q},\omega). \tag{34}$$

Taking into account the definition of the order parameter Eq. (4), we obtain the relation between the order parameter oscillations and the response functions $\eta^{(1(2))}$ at $\mathbf{q}\neq 0$:

$$\Delta_{1,\sigma}(\mathbf{q},\omega) = g\eta^{(1)}_\sigma(\mathbf{q},\omega), \quad \Delta_{2,\sigma}(\mathbf{q},\omega) = g\eta^{(2)}_\sigma(\mathbf{q},\omega), \tag{35}$$

where $g = V\Omega_0/4$ is the coupling constant.

Restricting with the linear response approximation we obtain from Eqs. (31), (33), (34), and (35) the following matrix equation:

$$\begin{pmatrix} e^{-1}\rho_{+,\sigma}(\mathbf{q},\omega) \\ -g^{-1}\Delta_{1,\sigma}(\mathbf{q},\omega) \\ -g^{-1}\Delta_{2,\sigma}(\mathbf{q},\omega) \\ e^{-1}\rho_{-,\sigma}(\mathbf{q},\omega) \end{pmatrix} = \begin{pmatrix} \Pi_{00}(\mathbf{q},\omega) & \Pi_{01}(\mathbf{q},\omega) & \Pi_{02}(\mathbf{q},\omega) & \Pi_{03}(\mathbf{q},\omega) \\ \Pi_{10}(\mathbf{q},\omega) & \Pi_{11}(\mathbf{q},\omega) & \Pi_{12}(\mathbf{q},\omega) & \Pi_{13}(\mathbf{q},\omega) \\ \Pi_{20}(\mathbf{q},\omega) & \Pi_{21}(\mathbf{q},\omega) & \Pi_{22}(\mathbf{q},\omega) & \Pi_{23}(\mathbf{q},\omega) \\ \Pi_{30}(\mathbf{q},\omega) & \Pi_{31}(\mathbf{q},\omega) & \Pi_{32}(\mathbf{q},\omega) & \Pi_{33}(\mathbf{q},\omega) \end{pmatrix} \begin{pmatrix} e\varphi_+(\mathbf{q},\omega)/2 \\ \Delta_{1,\sigma}(\mathbf{q},\omega) \\ \Delta_{2,\sigma}(\mathbf{q},\omega) \\ e\varphi_-(\mathbf{q},\omega)/2 \end{pmatrix}, \tag{36}$$

where the components of the polarization matrix are given by the expression

$$\Pi_{s_1s_2}(\mathbf{q},\omega) = \frac{1}{S}\sum_{\nu_1,\nu_2}\delta_{\mathbf{k}_1-\mathbf{q},\mathbf{k}_2}\Phi^{s_1s_2}_{\nu_1\nu_2}\frac{1+\lambda_1\lambda_2\cos(\chi_{\mathbf{k}_1}-\chi_{\mathbf{k}_2})}{2}\frac{f_{\nu_1}-f_{\nu_2}}{E_{\nu_1}-E_{\nu_2}-\hbar(\omega+i\gamma)}. \tag{37}$$

The factors $\Phi^{s_1s_2}_{\nu_1\nu_2}$ in Eq. (37) are expressed through the matrix (26):

$$\Phi^{s_1s_2}_{\nu_1\nu_2} = [\hat{M}^{(s_2)}(\mathbf{k}_1,\lambda_1,\mathbf{k}_2,\lambda_2)]_{i_{m_1},i_{m_2}}[\hat{M}^{(s_1)}(\mathbf{k}_2,\lambda_2,\mathbf{k}_1,\lambda_1)]_{i_{m_2},i_{m_1}} \tag{38}$$

[there is no summation over repeated indexes in Eq. (38)].

From Eq. (38) we obtain the following explicit expressions for $\Phi^{s_1s_2}_{\nu_1\nu_2}$:

$$\begin{aligned}
&\Phi^{00}_{\nu_1\nu_2} = \frac{1}{2}\left(1+\frac{\xi_1\xi_2+\Delta^2}{E_1E_2}\right), \quad \Phi^{01}_{\nu_1\nu_2} = -\frac{\Delta}{2}\left(\frac{1}{E_1}+\frac{1}{E_2}\right), \quad \Phi^{02}_{\nu_1\nu_2} = i\frac{\Delta}{2}\frac{\xi_2-\xi_1}{E_2E_1}, \quad \Phi^{03}_{\nu_1\nu_2} = \frac{1}{2}\left(\frac{\xi_2}{E_2}+\frac{\xi_1}{E_1}\right), \\
&\Phi^{11}_{\nu_1\nu_2} = \frac{1}{2}\left(1-\frac{\xi_1\xi_2-\Delta^2}{E_1E_2}\right), \quad \Phi^{12}_{\nu_1\nu_2} = \frac{i}{2}\left(\frac{\xi_1}{E_1}-\frac{\xi_2}{E_2}\right), \quad \Phi^{13}_{\nu_1\nu_2} = -\frac{\Delta}{2}\frac{\xi_1+\xi_2}{E_1E_2}, \\
&\Phi^{22}_{\nu_1\nu_2} = \frac{1}{2}\left(1-\frac{\xi_1\xi_2+\Delta^2}{E_1E_2}\right), \quad \Phi^{23}_{\nu_1\nu_2} = i\frac{\Delta}{2}\left(\frac{1}{E_2}-\frac{1}{E_1}\right), \\
&\Phi^{33}_{\nu_1\nu_2} = \frac{1}{2}\left(1+\frac{\xi_1\xi_2-\Delta^2}{E_1E_2}\right),
\end{aligned} \tag{39}$$

and $\Phi^{s_2,s_1}_{\nu_1\nu_2} = (\Phi^{s_1,s_2}_{\nu_1\nu_2})^*$. Here we use the notations $\xi_i \equiv \xi_{\nu_i}$ and $E_i \equiv E_{\nu_i}$.

Taking into account symmetry properties of the expression under summation in Eq. (37), one can show that some elements of the polarization matrix, namely, $\Pi_{01}(\mathbf{q},\omega)$, $\Pi_{02}(\mathbf{q},\omega)$, $\Pi_{03}(\mathbf{q},\omega)$, $\Pi_{10}(\mathbf{q},\omega)$, $\Pi_{20}(\mathbf{q},\omega)$, and $\Pi_{30}(\mathbf{q},\omega)$, are equal to zero exactly.

V. COLLECTIVE MODES

In the nonretarded approximation the scalar potential satisfies the Poisson equation

$$\nabla[\varepsilon(\mathbf{r})\nabla\varphi(\mathbf{r},t)] = -4\pi\rho(\mathbf{r},t), \tag{40}$$

where

$$\varepsilon(\mathbf{r}) = \begin{cases} 1, & z < -d/2, \\ \varepsilon, & -d/2 < z < d/2, \\ 1, & z > d/2 \end{cases} \tag{41}$$

is the space-dependent dielectric constant (we specify the case of two graphene layers separated by a dielectric layer with the dielectric constant ε and surrounded by a medium with $\varepsilon = 1$), d is the distance between graphene layers, and the z axis is directed perpendicular to graphene layers.

To obtain the eigenmode spectrum, we account for the charges induced in graphene layers by the scalar potential and

by the order parameter oscillations in Eq. (40):

$$\rho(\mathbf{r},t)=\sum_{\sigma}[\rho_{1,\sigma}(\mathbf{r}_{pl},t)\delta(z-d/2)+\rho_{2,\sigma}(\mathbf{r}_{pl},t)\delta(z+d/2)], \tag{42}$$

where $\mathbf{r}_{pl}$ is two-dimensional radius vector in the (x,y) plane.

Making the Fourier transformation of Eq. (40), we obtain the equation for $\varphi(\mathbf{q},z,\omega)$. Its solution yields the relation between the potentials $\varphi_{\pm}(\mathbf{q},\omega)=\varphi(\mathbf{q},d/2,\omega)\pm\varphi(\mathbf{q},-d/2,\omega)$ and the charge densities $\rho_{\pm}(\mathbf{q},\omega)=\sum_{\sigma}\rho_{\pm,\sigma}(\mathbf{q},\omega)$:

$$e^2\varphi_{\pm}(\mathbf{q},\omega)=V_{\pm}(q)\rho_{\pm}(\mathbf{q},\omega), \tag{43}$$

where

$$V_{\pm}(q)=\frac{4\pi e^2}{q}\frac{1\pm e^{-qd}}{(\varepsilon+1)\mp(\varepsilon-1)e^{-qd}} \tag{44}$$

are the Fourier-components of the Coulomb interaction energies $V_{\pm}(r_{pl})=V_{11}(r_{pl})\pm V_{12}(r_{pl})$. Here $V_{11}(r_{pl})$ and $V_{12}(r_{pl})$ are the energies of interaction of two electrons located in the same and different layers, correspondingly [we account for that in the uniform dielectric environment, $V_{11}(r_{pl})=V_{22}(r_{pl})$].

From Eqs. (36) and (43) we get the equation for the scalar potential and order parameter oscillations:

$$\begin{pmatrix} 2\Pi_{00}-\frac{2}{V_+(q)} & 0 & 0 & 0 & 0 & 0\\ 0 & \Pi_{11}+\frac{1}{g} & \Pi_{12} & 0 & 0 & \Pi_{13}\\ 0 & \Pi_{21} & \Pi_{22}+\frac{1}{g} & 0 & 0 & \Pi_{23}\\ 0 & 0 & 0 & \Pi_{11}+\frac{1}{g} & \Pi_{12} & \Pi_{13}\\ 0 & 0 & 0 & \Pi_{21} & \Pi_{22}+\frac{1}{g} & \Pi_{23}\\ 0 & \Pi_{31} & \Pi_{32} & \Pi_{31} & \Pi_{32} & 2\Pi_{33}-\frac{2}{V_-(q)} \end{pmatrix}\begin{pmatrix} e\varphi_+(\mathbf{q},\omega)/2\\ \Delta_{1,\uparrow}(\mathbf{q},\omega)\\ \Delta_{2,\uparrow}(\mathbf{q},\omega)\\ \Delta_{1,\downarrow}(\mathbf{q},\omega)\\ \Delta_{2,\downarrow}(\mathbf{q},\omega)\\ e\varphi_-(\mathbf{q},\omega)/2 \end{pmatrix}=0, \tag{45}$$

where $\Pi_{\alpha\beta}\equiv\Pi_{\alpha\beta}(\mathbf{q},\omega)$.

We calculate the polarization functions Eq. (37) in the Dirac approximation for the electron spectrum. In this approximation the sum over $\mathbf{k}$ is replaced with the integral over two separate circles in the Brillouin zone centered at the Dirac points K and K'. In these circles $|f(\mathbf{k})|\approx\hbar v_F k'$, and $\chi_{\mathbf{k}}\approx\mp\theta_{\mathbf{k}'}$, where $\mathbf{k}'$ is counted from the corresponding Dirac point, $\theta_{\mathbf{k}'}$ is the angle between $\mathbf{k}'$ and the x-axis, and v_F is the Fermi velocity in graphene. In the Dirac approximation the integrals in the expressions for $\Pi_{11}(\mathbf{q},\omega)$ and $\Pi_{22}(\mathbf{q},\omega)$ diverge at $k'\to\infty$. This divergence is unphysical one and emerges as a result of the approximations used. The same (unphysical) divergence emerges in the self-consistence equation (16) if it is evaluated in the Dirac approximation. Fortunately the quantities $\Pi_{11(22)}(\mathbf{q},\omega)+1/g$ that enter into Eq. (45) can be presented in a form that is free from such a divergence. Indeed Eq. (16) can be rewritten as

$$\frac{1}{g}=\frac{1}{S}\sum_{\mathbf{k},\lambda}\frac{1}{E_{\mathbf{k},\lambda}}\tanh\frac{E_{\mathbf{k},\lambda}}{2T}=-\frac{1}{S}\sum_{m,\mathbf{k},\lambda}\frac{f_{m,\mathbf{k},\lambda}-f_{-m,\mathbf{k},\lambda}}{E_{m,\mathbf{k},\lambda}-E_{-m,\mathbf{k},\lambda}}. \tag{46}$$

Using the relation (46) we get

$$\Pi_{ss}(\mathbf{q},\omega)+\frac{1}{g}=\Pi^{(R)}_{ss}(\mathbf{q},\omega)=\frac{1}{S}\sum_{\nu_1,\nu_2}\left[\delta_{\mathbf{k}_1-\mathbf{q},\mathbf{k}_2}\Phi^{ss}_{\nu_1\nu_2}\frac{1+\lambda_1\lambda_2\cos(\chi_{\mathbf{k}_1}-\chi_{\mathbf{k}_2})}{2}\frac{f_{\nu_1}-f_{\nu_2}}{E_{\nu_1}-E_{\nu_2}-\hbar(\omega+i\gamma)}\right.$$
$$\left.-\delta_{\mathbf{k}_1,\mathbf{k}_2}\delta_{m_1,-m_2}\delta_{\lambda_1,\lambda_2}\frac{f_{\nu_1}-f_{\nu_2}}{E_{\nu_1}-E_{\nu_2}}\right] \tag{47}$$

that do not diverge in the Dirac approximation [divergencies in $\Pi_{11(22)}$ and in Eq. (46) cancel each other].

Equating the determinant of the matrix in Eq. (45) to zero, we obtain the dispersion equation for the eigenmode spectrum. The determinant is factorized into three multipliers. The first multiplier yields the equation

$$\varepsilon_+(\mathbf{q},\omega)=1-V_+(q)\Pi_{00}(\mathbf{q},\omega)=0. \tag{48}$$

Equation (48) is the dispersion equation for the symmetric plasma excitation in the double layer system.

The dielectric function $\varepsilon_+(\mathbf{q},\omega)$ describes the screening of the scalar potential of a test charge $\rho^{\text{test}}_+(\mathbf{q},\omega)$:

$$e^2\varphi^{\text{scr}}_+(\mathbf{q},\omega)=\frac{V_+(q)}{\varepsilon_+(\mathbf{q},\omega)}\rho^{\text{test}}_+(\mathbf{q},\omega). \tag{49}$$

Equation (49) follows from Eq. (43) written in the form $e^2\varphi^{\text{scr}}_+(\mathbf{q},\omega)=V_+(q)[\rho^{\text{test}}_+(\mathbf{q},\omega)+\rho^{\text{ind}}_+(\mathbf{q},\omega)]$, where $\rho^{\text{ind}}_+(\mathbf{q},\omega)=e^2\Pi_{00}(\mathbf{q},\omega)\varphi^{\text{scr}}_+(\mathbf{q},\omega)$ is the induced charge.

From the continuity equation for the charge we obtain the relation between the polarization function $\Pi_{00}(\mathbf{q},\omega)$ and the longitudinal parallel current conductivity $\sigma_{+,xx}(\mathbf{q},\omega)$:

$$\sigma_{+,xx}(q\mathbf{i}_x,\omega)=\frac{ie^2\omega}{q^2}\Pi_{00}(q\mathbf{i}_x,\omega), \tag{50}$$

where $\mathbf{i}_x$ is the unit vector along the x axis.

Considering the Maxwell's equations with the corresponding boundary conditions and the matter equation for the current, one can get the following dispersion equation for the

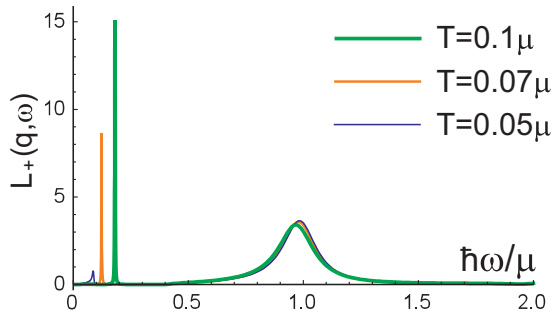

FIG. 2. Frequency dependence of the dielectric loss function (52) at $T = 0.1\mu,\ 0.07\mu,\ 0.05\mu$, $q = 0.1k_F$, $\Delta = 0.2\mu$, and $\hbar\gamma = 10^{-3}\mu$.

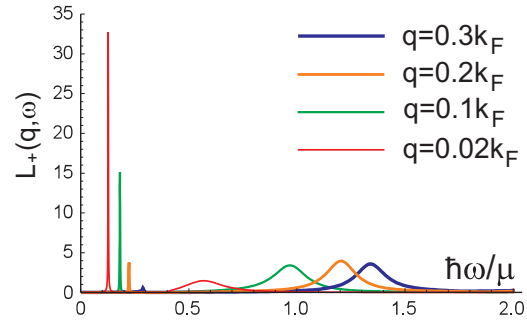

FIG. 3. Frequency dependence of the dielectric loss function (52) at $T = 0.1\mu$, $q = 0.02k_F,\ 0.1k_F,\ 0.2k_F,\ 0.3k_F$, $\Delta = 0.2\mu$, and $\hbar\gamma = 10^{-3}\mu$.

symmetric plasmon modes [32,37]:

$$1 + \frac{4\pi i\kappa_1}{\omega}\sigma_{+,xx}(q\mathbf{i}_x, \omega) + \frac{\varepsilon\kappa_1}{\kappa_2}\tanh\frac{\kappa_2 d}{2} = 0, \tag{51}$$

where $\kappa_1 = \sqrt{q^2 - \omega^2/c^2}$ and $\kappa_2 = \sqrt{q^2 - \varepsilon\omega^2/c^2}$. Equation (51) accounts for retarded effects, and due to this it differs from Eq. (48). In the limit $\kappa_1 = \kappa_2 = q$ that corresponds to nonretarded (plasmon) approximation, Eq. (51) is reduced to Eq. (48).

Thus, we have shown that the order parameter oscillations are decoupled from the oscillations of φ_+ and do not influence the spectrum of symmetric plasmon modes. The same result was obtained in Ref. [32] based on the observation that the generalized Ward identity for the vertex function $\Gamma_{\mu,+}$ is satisfied with bare vertexes (the vertexes $\Gamma_{\mu,+}$ describe interaction of electrons with φ_+ and $\mathbf{A}_+$, the sum of vector potentials of two layers). Therefore the Feynman diagram with the bare vertexes (which do not account for order parameter oscillations) gives a gauge invariant polarization function Π_{00}. The gauge invariance of Π_{00} can be also checked directly (see the Appendix).

In the general case Eq. (48) has two solutions [32]: one is below the gap ($\hbar\omega < 2\Delta$) and the other is above the gap ($\hbar\omega > 2\Delta$). It can be seen from the frequency dependence of the dielectric loss function. This function is defined as

$$L_+(\mathbf{q}, \omega) = -\mathrm{Im}\left[\frac{1}{\varepsilon_+(\mathbf{q}, \omega)}\right]. \tag{52}$$

It determines relative losses of energy of oscillations of a test charge ρ_+^{test}. The positions of peaks in the ω dependence of $L_+(q, \omega)$ at fixed q correspond to the eigenmode frequencies. A half-width of the peak at its half-height gives the damping rate for the corresponding mode.

To compare the properties of symmetric and antisymmetric (see below) modes it is instructive to illustrate changes in the frequency dependence of $L_+(\mathbf{q}, \omega)$ under variation of temperature (Fig. 2) and the wave vector (Fig. 3). One can see that the peak that corresponds to the lower mode disappears at small T and for large q. One can also see in Figs. 2 and 3 a wide peak that corresponds to the upper (strongly damped) mode. Note that at $\Delta \to 0$ the damping rate of the upper mode decreases, and this mode is transformed into the normal state optical plasmon mode.

The second multiplier in the determinant of the matrix in Eq. (45) yields the equation

$$\Pi_{11}^{(R)}(\mathbf{q}, \omega)\Pi_{22}^{(R)}(\mathbf{q}, \omega) + [\Pi_{12}(\mathbf{q}, \omega)]^2 = 0. \tag{53}$$

It is the dispersion equation for the excitations where only the difference $\Delta_\uparrow - \Delta_\downarrow$ oscillates. Such oscillations are decoupled from the scalar potential oscillations.

In the theory of superconductivity the eigenmodes that correspond to oscillations of the phase and the modulus of the order parameter are known as the Anderson-Bogoliubov (AB) mode [38,39] and the Schmid [40] mode. Since in common superconductors the oscillations of the phase of the order parameter are coupled to plasma (scalar potential) oscillations, a genuine Anderson-Bogoliubov mode can emerge in neutral Fermi superfluids. In double layer systems with electron-hole pairing the presence of two superconducting components allows us to realize the AB mode. To visualize the AB and the Schmid modes we introduce the functions

$$L_{11}(\mathbf{q}, \omega) = \frac{1}{g}\mathrm{Im}\left[\frac{1}{\Pi_{11}^{(R)}(\mathbf{q}, \omega) + \frac{[\Pi_{12}(\mathbf{q},\omega)]^2}{\Pi_{22}^{(R)}(\mathbf{q},\omega)}}\right], \tag{54}$$

$$L_{22}(\mathbf{q}, \omega) = \frac{1}{g}\mathrm{Im}\left[\frac{1}{\Pi_{22}^{(R)}(\mathbf{q}, \omega) + \frac{[\Pi_{12}(\mathbf{q},\omega)]^2}{\Pi_{11}^{(R)}(\mathbf{q},\omega)}}\right]. \tag{55}$$

These functions can be interpreted as analogs of the energy loss function (52). The functions L_{11} and L_{22} describe losses of energy under externally driven oscillations of the amplitude and the phase of the order parameter, respectively.

The frequency dependencies of $L_{11}(\mathbf{q}, \omega)$ and $L_{22}(\mathbf{q}, \omega)$ at three different q and $T = 0.1\mu$ are shown in Fig. 4. One can see that the function $L_{22}(\mathbf{q}, \omega)$, Fig. 4(b), has a peak at $\hbar\omega < 2\Delta$. The function $L_{11}(\mathbf{q}, \omega)$, Fig. 4(a), has two peaks: one is at $\hbar\omega < 2\Delta$ (at the same frequency as the peak in Fig. 4(b)) and the other at $\hbar\omega > 2\Delta$. Two peaks in Fig. 4(a) appear due to the coupling of oscillations of the amplitude and the phase of the order parameter (in conventional superconductors these oscillations are decoupled from each other [36]). In Fig. 5 we present the same dependencies as in Fig. 4 at $T = 0$. One can see that the positions of the peaks remain practically unchanged under lowering of temperature (at $\Delta = \mathrm{const}$). At the same time an essential narrowing of the low-frequency

peak at $T = 0$ signals a decrease of the damping rate of the lower mode. It is connected with the fact that the Landau damping in the frequency domain $\hbar\omega < 2\Delta$ is proportional to $\exp(-\Delta/T)$. In contrast, in the frequency domain $\hbar\omega > 2\Delta$ the Landau damping remains strong even at $T = 0$. Therefore the high-frequency peak is not changed under lowering of temperature.

The spectra of the modes determined by Eq. (53) are shown in Fig. 6. The dependencies presented are obtained from the position of the maximum of the functions (54) and (55) at $T = 0$. At small wave vectors the dispersion relation for the lower mode is approximated by the expression $\omega = qv_F/\sqrt{2}$, that is the spectrum of the AB mode in two dimensions. At large q the frequency of this mode approaches $\omega = 2\Delta/\hbar$. The frequency of the upper mode approaches $2\Delta/\hbar$ at $q \to 0$. This mode can be recognized only in the limit $q/k_F \ll 1$. At $q/k_F \gtrsim 0.2$ the peak that corresponds to that mode washes out. The lower mode in Fig. 6 should be interpreted as an analog of the AB mode, and the upper mode as the analog of the Schmid mode.

The third multiplier in the determinant of the matrix in Eq. (45) yields the equation

$$\left[\Pi_{11}^{(R)}(\mathbf{q},\omega)\Pi_{22}^{(R)}(\mathbf{q},\omega) + [\Pi_{12}(\mathbf{q},\omega)]^2\right][1 - V_-(q)\Pi_{33}(\mathbf{q},\omega)] - V_-(q)\Big[\Pi_{11}^{(R)}(\mathbf{q},\omega)[\Pi_{23}(\mathbf{q},\omega)]^2 - \Pi_{22}^{(R)}(\mathbf{q},\omega)[\Pi_{13}(\mathbf{q},\omega)]^2 + 2\Pi_{12}(\mathbf{q},\omega)\Pi_{13}(\mathbf{q},\omega)\Pi_{23}(\mathbf{q},\omega)\Big] = 0. \tag{56}$$

One can see that at $V_-(q) = 0$ (that corresponds to $d = 0$), Eq. (56) coincides with Eq. (53).

At $V_-(q) \neq 0$ Eq. (56) can be rewritten in the form

$$\varepsilon_-(\mathbf{q},\omega) = 1 - V_-(q)\Pi_-(\mathbf{q},\omega) = 0, \tag{57}$$

where

$$\Pi_-(\mathbf{q},\omega) = \Pi_{33}(\mathbf{q},\omega) + \frac{\Pi_{11}^{(R)}(\mathbf{q},\omega)[\Pi_{23}(\mathbf{q},\omega)]^2 - \Pi_{22}^{(R)}(\mathbf{q},\omega)[\Pi_{13}(\mathbf{q},\omega)]^2 + 2\Pi_{12}(\mathbf{q},\omega)\Pi_{13}(\mathbf{q},\omega)\Pi_{23}(\mathbf{q},\omega)}{\Pi_{11}^{(R)}(\mathbf{q},\omega)\Pi_{22}^{(R)}(\mathbf{q},\omega) + [\Pi_{12}(\mathbf{q},\omega)]^2}. \tag{58}$$

The function $\Pi_-(\mathbf{q},\omega)$ can be understood as the polarization function "dressed" by the order parameter oscillations. Numerical evaluation confirms the gauge invariance of the function (58) in the limit $\gamma \to 0$ (see the Appendix).

Equation (57) is the dispersion equation for antisymmetric plasma oscillations coupled to the order parameter oscillations. The dielectric function $\varepsilon_-(\mathbf{q},\omega)$ determines screening of the scalar potential of a test charge ρ_-^{test}: $e^2\varphi_-^{\text{scr}}(\mathbf{q},\omega) = V_-(q)\rho_-^{\text{test}}(\mathbf{q},\omega)/\varepsilon_-(\mathbf{q},\omega)$.

The relation between the polarization function $\Pi_-(\mathbf{q},\omega)$ and the counterflow conductivity is given by the equation

$$\sigma_{-,xx}(q\mathbf{i}_x,\omega) = \frac{ie^2\omega}{q^2}\Pi_-(q\mathbf{i}_x,\omega). \tag{59}$$

Using the condition of the gauge invariance (A5) and the expressions (A3) and (A4) in the Appendix, one can show

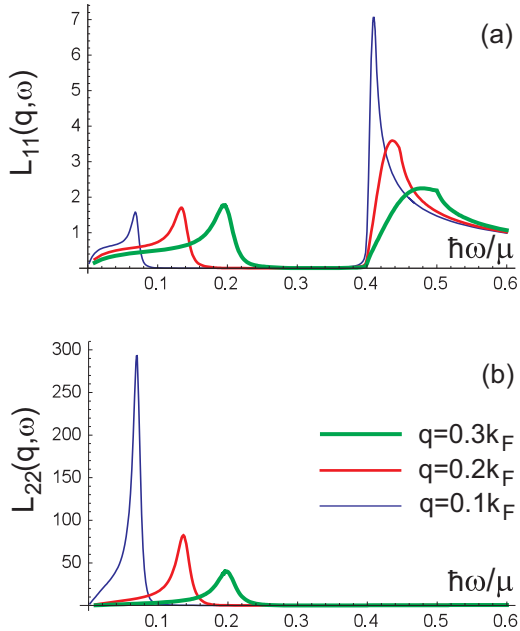

FIG. 4. Frequency dependence of the energy loss functions (54), (55) in μ/gk_F^2 units at $T = 0.1\mu$, $q = 0.1k_F$, $0.2k_F$, $0.3k_F$, $\Delta = 0.2\mu$, and $\hbar\gamma = 10^{-3}\mu$.

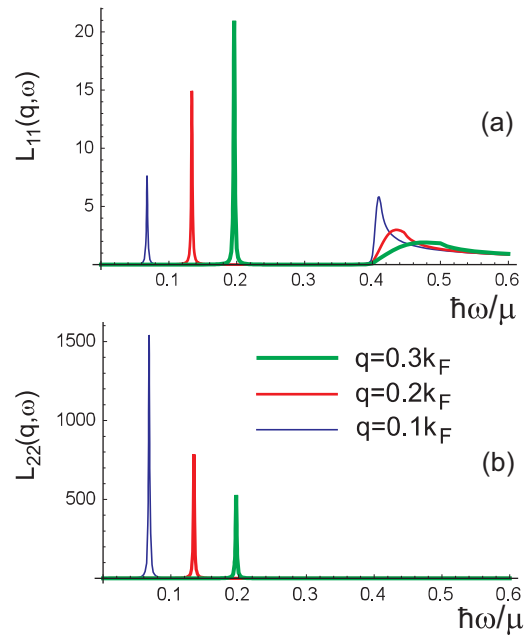

FIG. 5. The same as in Fig. 4 at $T = 0$.

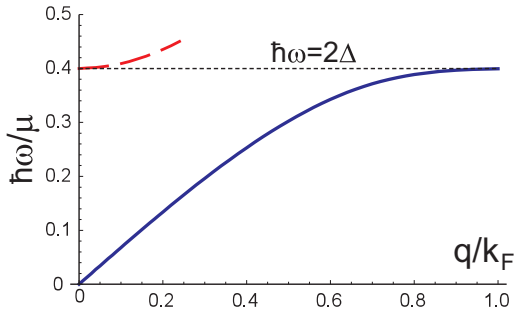

FIG. 6. The spectra of the Anderson-Bogoliubov (solid curve) and Schmid (dashed curve) modes in the double layer graphene system.

that at small q the quantity $\Pi_-(q\mathbf{i}_x, \omega) \propto q^2$. Therefore the conductivity $\sigma_{-,xx}(q\mathbf{i}_x, \omega)$ given by Eq. (59) is finite at $q \to 0$. Also from the physical reasons the real part of $\sigma_{-,xx}(q\mathbf{i}_x, \omega)$ should be positive. We have checked numerically the fulfillment of the latter condition.

The dispersion equation for the antisymmetric (acoustic) plasmon mode that accounts for retarded effects has the form [32,37]

$$\left(1 + \frac{4\pi i\kappa_1\sigma_{-,xx}(q\mathbf{i}_x, \omega)}{\omega}\right)\tanh\frac{\kappa_2 d}{2} + \frac{\varepsilon\kappa_1}{\kappa_2} = 0. \qquad (60)$$

In the nonretarded approximation ($\kappa_1 = \kappa_2 = q$) Eq. (60) reduces to Eq. (57).

We analyze Eq. (57) considering the energy loss function

$$L_-(\mathbf{q}, \omega) = -\mathrm{Im}\left[\frac{1}{\varepsilon_-(\mathbf{q}, \omega)}\right]. \qquad (61)$$

The frequency dependencies of $L_-(\mathbf{q}, \omega)$ at four different wave vectors ($q = 0.2k_F$, $0.4k_F$, $0.6k_F$, $0.8k_F$), $\Delta = 0.2\mu$, $T = 0.1\mu$, and $T = 0$ are shown in Fig. 7. The parameters used for the calculations are $\varepsilon = 4$, $dk_F = 0.1$, and $\hbar\gamma = 10^{-3}\mu$. One can see that in similarity with $L_+(\mathbf{q}, \omega)$ the function $L_-(\mathbf{q}, \omega)$ contains two peaks: one is below the gap 2Δ and the other is above the gap. The low-frequency peak is narrower than the high-frequency one. Differently from the $L_+(\mathbf{q}, \omega)$ dependence, the position of the lower peak of the $L_-(\mathbf{q}, \omega)$ dependence remains practically unchanged under variation of temperature (at $\Delta = \mathrm{const}$). This peak does not disappear at $T = 0$.

In conventional superconductors the mode that corresponds to coupled oscillations of the scalar potential and the phase of the order parameter is known as the Carlson-Goldman (CG) mode [41]. The frequency of the CG mode satisfies the inequality $\hbar\omega < 2\Delta$. The mentioned similarities allow us to interpret the lower antisymmetric mode as an analog of the Carlson-Goldman mode.

Lowering of temperature results in a considerable decrease of the damping rate of the lower mode but does not influence the damping rate of the upper mode. As in the case of the AB and Schmid modes, it is connected with the specific temperature and frequency dependence of the Landau damping in the state with electron-hole pairing [32].

The dispersion curves calculated from the positions of two maxima of the function (61) at $T = 0$ are shown in Fig. 8.

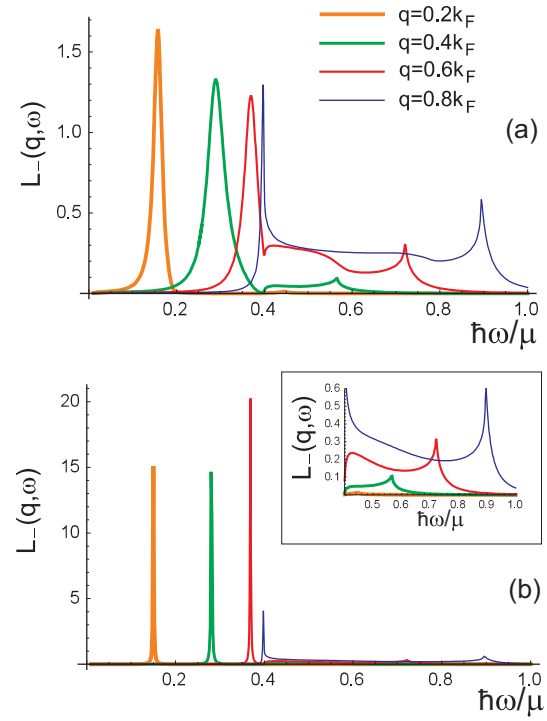

FIG. 7. Frequency dependence of the energy loss function (61) at $T = 0.1\mu$ (a) and $T = 0$ (b). The high-frequency peaks at $T = 0$ are shown in the inset in another scale.

The lower mode has the acoustic dispersion relation at small wave vectors. At large q its frequency approaches $2\Delta/\hbar$. The dispersion curve for the acoustic plasmon mode in the normal state ($\Delta = 0$) calculated at the same parameters is also shown in Fig. 8. It is known [42] that the velocity v_a of the acoustic plasmon in a double-layer graphene system can be very close to v_F, but it is always larger than v_F irrespective of the values of d and ε. For ε and d specified above $v_a \approx 1.016v_F$. The velocity of the CG mode v_{CG} can be smaller than v_F. In our case $v_{CG} \approx 0.77v_F$. The velocity v_{CG} is larger than the velocity of the AB mode $v_{AB} = v_F/\sqrt{2}$ but there is no requirement for v_{CG} to be larger than v_F. It is correlated with the fact that in the normal state the mode with the phase velocity $v_{ph} < v_F$ should experience strong Landau

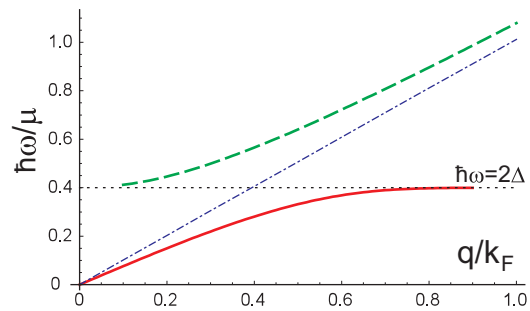

FIG. 8. The dispersion curves for the Carlson-Goldman mode (solid curve) and for the upper antisymmetric plasmon mode (dashed curve). The spectrum of the antisymmetric (acoustic) plasmon mode in the normal state is shown by the dash-dotted line.

damping, but in the paired state the modes with $\hbar\omega < 2\Delta$ do not experience Landau damping at $T = 0$.

At $q/k_F > 0.9$ the peak at the $L_-(\mathbf{q}, \omega)$ dependence that corresponds to the CG mode disappears. In contrast, the upper mode peak is well recognized at large q, while at small q this peak almost disappears. At $\Delta \to 0$ the upper mode is transformed into the acoustic plasmon mode. It allows us to interpret the upper antisymmetric mode as a residual acoustic plasmon mode.

It is instructive to compare the CG mode in conventional superconductors and in counterflow superconductors. Under the two-fluid picture, the CG mode is regarded as out-of-phase motion of the superfluid and normal components. In conventional s-wave superconductors the CG mode can be observed only at a temperature close to the critical temperature T_c [36,43]. At such temperatures the density of the normal component is comparable to the density of the superfluid component. But in clean s-wave superconductors at T close to T_c the CG mode is smeared out due to the Landau damping of the quasiparticles, and it can be clearly seen only in dirty systems [43]. In d-wave superconductors, due to the presence of four Fermi points at the nodes of the d-wave order parameter the CG mode can be registered in clean systems and it survives at much lower temperatures, down to $T \sim 0.1T_c$ [44,45]. The CG mode was also predicted for a color-flavor locked (CFL) phase of color superconducting dense quark matter [46]. The presence of two different types of quarks with nonequal gaps in the CFL phase causes a partial suppression of the Landau damping. As a consequence, the CG mode can be observed in the pure limit at temperature close to the critical one ($T/T_c \geqslant 0.986$) [46]. The situation in counterflow superconductors differs from ones in s-wave and d-wave superconductors and for a CFL phase of superconducting quark matter. In the counterflow superconductors the CG mode can be interpreted as in-phase motion of the superfluid and normal components, and due to that the CG mode can be observed at all temperatures below the critical one, in particular at $T = 0$ (Fig. 8). At low temperature the Landau damping is suppressed. Therefore we consider pure counterflow superconductors as more appropriate for the observation of the CG mode.

In this study we consider the contact pairing potential. For more careful analysis the contact potential should be replaced with a screened Coulomb potential. In this case one should take into account a dependence of the order parameter on the momentum (see Sec. II). To describe the state with the momentum-dependent order parameter, one can approximate the screened Coulomb interaction by a function which is separable in the incoming and outgoing momenta, as was done in Refs. [17,47]. Restricting with the separable pairing potential and considering the close-band pairing (the pairing of carriers in the conduction band in layer 1 with carriers in the valence band in layer 2), we arrive at the polarization functions with the additional momentum dependent factor under the integral over $\mathbf{k}$. Similar factor emerges in the polarization functions for d-wave superconductors [44] (in the latter case this factor is angle dependent). Evaluating the polarization functions with the additional factor, we obtain dispersion curves that are very close to ones obtained for the model with the contact pairing potential. It can be understood as follows. The collective mode spectra presented in Figs. 6 and 8 are determined in the main part by two parameters: the Fermi velocity v_F and the gap in the quasiparticle spectrum 2Δ. The parameter 2Δ is sensitive to the form of the pairing potential, and it depends on the interlayer distance and on the density of the carriers. But in our study we do not evaluate this parameter. We just fix its value. If the parameter 2Δ is fixed, accounting for a momentum dependence of the order parameter does not influence significantly the collective mode spectrum. Thus we conclude that the model with the contact pairing potential adequately describes collective modes in counterflow superconductors.

VI. CONCLUSION

In conclusion, we have shown that explicit accounting for the order parameter oscillations is crucial in obtaining the spectra of antisymmetric plasma modes in double layer systems with electron-hole pairing. At the same time the approach [32] based on a particular solution of the generalized Ward identity cannot describe a number of important features. In particular, taking into account the order parameter oscillations, we predict the existence of two antisymmetric modes. The upper mode can be interpreted as a residual normal state acoustic plasmon, and the lower mode as an analog of the Carlson-Goldman mode. Two more modes interpreted as analogs of the Anderson-Bogoliubov and Schmid modes are also identified. The latter modes are associated with out-of-phase oscillations of the order parameters of two spin subsystems.

While the results are obtained with reference to a double monolayer graphene, one can expect that they reflect the general collective mode behavior in double layer systems with electron-hole pairing. Our approach can be easily extended to the double bilayer graphene systems [20,21]. The polarization functions for the double bilayer graphene are obtained from Eq. (37) under substitutions $\xi_{\mathbf{k},\lambda} \approx \lambda\hbar^2 k'^2/2m - \mu$ and $\chi_{\mathbf{k}} \approx \mp 2\theta_{\mathbf{k}'}$, where m is the effective mass. Preliminary calculations show that the collective mode systematics for the double bilayer graphene systems is the same as for the double monolayer ones. At the same time we emphasize that our approach is not applied to the systems with low density of carriers and a large gap between the valence and conduction bands. The counterflow superconductivity in the low density limit is described by the interacting boson model [24,48,49]. Such systems also have two superfluid components but the frequency of the mode that corresponds to out-of-phase oscillations of two components becomes imaginary-valued under increase of the interlayer distance [24,49]. It signals an instability with respect to spatial separation of the components. The system considered in the present paper does not show softening of the out-of-phase mode and it is stable with respect to spatial separation.

ACKNOWLEDGMENT

This study was supported by a Grant of the Ukraine State Fund for Fundamental Research (Project No. 33683).

APPENDIX: GAUGE INVARIANCE OF THE POLARIZATION FUNCTIONS

Assuming that the x components of the vector potential $\mathbf{A}_\pm = \mathbf{A}_1 \pm \mathbf{A}_2$ are nonzero, one can obtain the following expression for the charge density oscillations:

$$\rho_\pm(q\mathbf{i}_x,\omega) = e^2[\Pi_{\pm,0}(q\mathbf{i}_x,\omega)\varphi_\pm(q\mathbf{i}_x,\omega) + \Pi_{\pm,x}(q\mathbf{i}_x,\omega)A_{\pm,x}(q\mathbf{i}_x,\omega)]. \tag{A1}$$

Here $\Pi_{+,0}(\mathbf{q},\omega) \equiv \Pi_{00}(\mathbf{q},\omega)$ and $\Pi_{-,0}(\mathbf{q},\omega) \equiv \Pi_{-}(\mathbf{q},\omega)$ are the polarization functions given by Eqs. (37) and (58). The functions $\Pi_{\pm,x}(q\mathbf{i}_x,\omega)$ in Eq. (A1) describe the response to the vector potential (the interaction with the vector potential is given by the Hamiltonian $H_A = -(1/2c)\int d\mathbf{r}[j_{+,x}A_{+,x} + j_{-,x}A_{-,x}]$). The explicit expressions for these quantities are the following:

$$\Pi_{+,x}(\mathbf{q},\omega) = \frac{1}{S}\sum_{\nu_1,\nu_2}\delta_{\mathbf{k}_1-\mathbf{q},\mathbf{k}_2}\Phi^{03}_{\nu_1\nu_2}\frac{\lambda_1\cos\chi_{\mathbf{k}_1}+\lambda_2\cos\chi_{\mathbf{k}_2}}{2} \times \frac{f_{\nu_1}-f_{\nu_2}}{E_{\nu_1}-E_{\nu_2}-\hbar(\omega+i\gamma)} \tag{A2}$$

and

$$\Pi_{-,x}(\mathbf{q},\omega) = \frac{v_F}{c}\left[\Pi_{33,x} - \frac{\Pi_{31,x}\left[\Pi_{13}\Pi^{(R)}_{22}-\Pi_{12}\Pi_{23}\right]+\Pi_{32,x}\left[\Pi_{23}\Pi^{(R)}_{11}-\Pi_{21}\Pi_{13}\right]}{\Pi^{(R)}_{11}\Pi^{(R)}_{22}-\Pi_{12}\Pi_{21}}\right], \tag{A3}$$

where the functions $\Pi_{ss'}(\mathbf{q},\omega)$ and $\Pi^{(R)}_{ss}(\mathbf{q},\omega)$ are given by Eqs. (37), (47), and

$$\Pi_{3s,x}(\mathbf{q},\omega) = \frac{1}{S}\sum_{\nu_1,\nu_2}\delta_{\mathbf{k}_1-\mathbf{q},\mathbf{k}_2}\Phi^{s0}_{\nu_1\nu_2}\frac{\lambda_1\cos\chi_{\mathbf{k}_1}+\lambda_2\cos\chi_{\mathbf{k}_2}}{2} \times \frac{f_{\nu_1}-f_{\nu_2}}{E_{\nu_1}-E_{\nu_2}-\hbar(\omega+i\gamma)} \tag{A4}$$

$(s = 1, 2, 3)$.

The gauge invariance requires that

$$\omega\Pi_{\pm,0}(q\mathbf{i}_x,\omega) - qv_F\Pi_{\pm,x}(q\mathbf{i}_x,\omega) = 0. \tag{A5}$$

Numerical evaluation of the left-hand part of (A5) with the upper as well as with the lower sign shows that it goes to zero at $\gamma \to 0$. Thus we conclude that in the pure limit our approach yields the gauge invariant polarization functions.

[1] S. I. Shevchenko, Fiz. Nizk. Temp. **2**, 505 (1976) [Sov. J. Low Temp. Phys. 2, 251 (1976)].
[2] Yu. E. Lozovik and V. I. Yudson, Zh. Eksp. Teor. Fiz. **71**, 738 (1976) [Sov. Phys. JETP 44, 389 (1976)].
[3] D. V. Fil and S. I. Shevchenko, Fiz. Nizk. Temp. **44**, 1111 (2018) [Low Temp. Phys. **44**, 867 (2018)].
[4] M. Kellogg, J. P. Eisenstein, L. N. Pfeiffer, and K. W. West, Phys. Rev. Lett. **93**, 036801 (2004).
[5] E. Tutuc, M. Shayegan, and D. A. Huse, Phys. Rev. Lett. **93**, 036802 (2004).
[6] R. D. Wiersma, J. G. S. Lok, S. Kraus, W. Dietsche, K. von Klitzing, D. Schuh, M. Bichler, H.-P. Tranitz, and W. Wegscheider, Phys. Rev. Lett. **93**, 266805 (2004).
[7] J. P. Eisenstein, Annu. Rev. Condens. Matter Phys. **5**, 159 (2014).
[8] I. B. Spielman, J. P. Eisenstein, L. N. Pfeiffer, and K. W. West, Phys. Rev. Lett. **87**, 036803 (2001).
[9] D. Nandi, A. D. K. Finck, J. P. Eisenstein, L. N. Pfeiffer, and K. W. West, Nature (London) **488**, 481 (2012).
[10] A. F. Croxall, K. Das Gupta, C. A. Nicoll, M. Thangaraj, H. E. Beere, I. Farrer, D. A. Ritchie, and M. Pepper, Phys. Rev. Lett. **101**, 246801 (2008).
[11] J. A. Seamons, C. P. Morath, J. L. Reno, and M. P. Lilly, Phys. Rev. Lett. **102**, 026804 (2009).
[12] A. Gamucci, D. Spirito, M. Carrega, B. Karmakar, A. Lombardo, M. Bruna, L. N. Pfeiffer, K. W. West, A. C. Ferrari, M. Polini, and V. Pellegrini, Nat. Commun. **5**, 5824 (2014).
[13] G. W. Burg, N. Prasad, K. Kim, T. Taniguchi, K. Watanabe, A. H. MacDonald, L. F. Register, and E. Tutuc, Phys. Rev. Lett. **120**, 177702 (2018).
[14] Yu. E. Lozovik and A. A. Sokolik, Pis'ma Zh. Eksp. Teor. Fiz. **87**, 61 (2008) [JETP Lett. **87**, 55 (2008)].
[15] H. Min, R. Bistritzer, J.-J. Su, and A. H. MacDonald, Phys. Rev. B **78**, 121401(R) (2008).
[16] B. Seradjeh, H. Weber, and M. Franz, Phys. Rev. Lett. **101**, 246404 (2008).
[17] M. P. Mink, H. T. C. Stoof, R. A. Duine, and A. H. MacDonald, Phys. Rev. B **84**, 155409 (2011).
[18] I. Sodemann, D. A. Pesin, and A. H. MacDonald, Phys. Rev. B **85**, 195136 (2012).
[19] Yu. E. Lozovik, S. L. Ogarkov, and A. A. Sokolik, Phys. Rev. B **86**, 045429 (2012).
[20] A. Perali, D. Neilson, and A. R. Hamilton, Phys. Rev. Lett. **110**, 146803 (2013).
[21] J.-J. Su and A. H. MacDonald, Phys. Rev. B **95**, 045416 (2017).
[22] S. Conti, A. Perali, F. M. Peeters, and D. Neilson, Phys. Rev. Lett. **119**, 257002 (2017).
[23] M. Zarenia, A. Perali, D. Neilson, and F. M. Peeters, Sci. Rep. **4**, 7319 (2014).
[24] F. C. Wu, F. Xue, and A. H. MacDonald, Phys. Rev. B **92**, 165121 (2015).
[25] B. Debnath, Y. Barlas, D. Wickramaratne, M. R. Neupane, and R. K. Lake, Phys. Rev. B **96**, 174504 (2017).
[26] O. L. Berman and R. Ya. Kezerashvili, Phys. Rev. B **96**, 094502 (2017).

[27] O. L. Berman, G. Gumbs, and R. Ya. Kezerashvili, Phys. Rev. B **96**, 014505 (2017).
[28] S. Saberi-Pouya, M. Zarenia, A. Perali, T. Vazifehshenas, and F. M. Peeters, Phys. Rev. B **97**, 174503 (2018).
[29] B. Seradjeh, J. E. Moore, and M. Franz, Phys. Rev. Lett. **103**, 066402 (2009).
[30] D. K. Efimkin, Yu. E. Lozovik, and A. A. Sokolik, Phys. Rev. B **86**, 115436 (2012).
[31] K. V. Germash and D. V. Fil, Phys. Rev. B **91**, 115442 (2015).
[32] K. V. Germash and D. V. Fil, Phys. Rev. B **93**, 205436 (2016).
[33] K. V. Germash and D. V. Fil, Europhys. Lett. **118**, 67008 (2017).
[34] Y. Nambu, Phys. Rev. **117**, 648 (1960).
[35] J. R. Schrieffer, *Theory of Superconductivity* (Benjamin, New York, 1964).
[36] I. O. Kulik, O. Entin-Wohlman, and R. Orbach, J. Low Temp. Phys. **43**, 591 (1981).
[37] Yu.V. Bludov, A. Ferreira, N. M. R. Peres, and M. I. Vasilevskiy, Int. J. Mod. Phys. B **27**, 1341001 (2013).
[38] P. W. Anderson, Phys. Rev. **112**, 1900 (1958).
[39] N. N. Bogoljubov, V. V. Tolmachov, and D. V. Shirkov, Fortschr. Phys. **6**, 605 (1958).
[40] A. Schmid, Phys. Kondens. Materie **8**, 129 (1968).
[41] R. V. Carlson and A. M. Goldman, Phys. Rev. Lett. **34**, 11 (1975).
[42] R. E. V. Profumo, R. Asgari, M. Polini, and A. H. MacDonald, Phys. Rev. B **85**, 085443 (2012).
[43] Y. Ohashi and S. Takada, J. Phys. Soc. Jpn. **66**, 2437 (1997).
[44] Y. Ohashi and S. Takada, Phys. Rev. B **62**, 5971 (2000).
[45] S. G. Sharapov and H. Beck, Phys. Rev. B **65**, 134516 (2002).
[46] V. P. Gusynin and I. A. Shovkovy, Nucl. Phys. A **700**, 577 (2002).
[47] Y. E. Lozovik and A. A. Sokolik, Eur. Phys. J. B **73**, 195 (2010).
[48] Yu. E. Lozovik and O. L. Berman, Zh. Eksp. Teor. Fiz. **111**, 1879 (1997) [J. Exp. Theor. Phys. **84**, 1027 (1997)].
[49] D. V. Fil and S. I. Shevchenko, Fiz. Nizk. Temp. **42**, 1013 (2016) [Low Temp. Phys. **42**, 794 (2016)].